Design of a Flexible, Wearable Interdigitated Capacitive Sensor for Monitoring Biomarkers of Atopic Dermatitis

Alexandar R. Todorov, Krittika Goyal, Russel N. Torah, Mahmoud Wagih, *Member, IEEE*, Michael R. Ardern-Jones, Steven W. Day, Stephen P. Beeby, *Fellow, IEEE*

***Abstract*— The emergence of wearable and remote sensing devices in e-health has revolutionized personalized healthcare monitoring, but the field of dermatology has yet to witness significant progress in this area. The diagnosis and monitoring of atopic dermatitis (AD), a common skin disease causing inflammation and rashes, depend on in-person assessment, leading to subjective evaluations and treatment procedures. This work presents a novel interdigitated capacitive (IDC) sensor, specifically designed to detect biomarkers of AD and to empirically estimate the severity of the condition. The design was proven by finite element analysis software to detect only biomarkers of AD – dehydration of the outermost skin layer. The IDC sensor has a compact and flexible footprint (sensing area of around 40 mm^2), it is compatible with a wearable and non-invasive system, and can be used to remotely gather localized data about the condition. To calibrate its measurements a novel hydration-gradient skin-mimicking phantom was developed, which simulates varying skin hydration conditions on the same substrate. The sensor is compared against a commercial skin hydration device and its sensitivity is mapped against the arbitrary units of the commercial device, resulting in a normalized capacitance sensitivity of 13.1 pF/cm^2 per 1 A.U. This novel IDC sensor is the first sensor to accurately measure the permittivity of specific layers of the skin. Its bespoke design is the main enabler of the outermost layer's permittivity to be isolated from the skin. This presents promising prospects for remote patient care, enabling accurate diagnosis, treatment monitoring, and personalized interventions for AD.**

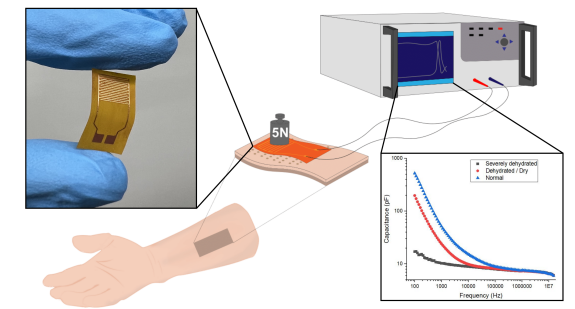

***Index Terms*— interdigitated sensors, interdigitated capacitors, skin hydration, flexible wearable sensors, atopic dermatitis, skin phantom, stratum corneum permittivity**

I. Introduction

In recent years, there has been a growing focus on developing wearable and remote sensing devices for personalized, in-home healthcare monitoring [1]. This has been driven by advances in information and communication technologies, commonly referred to as "e-health" or digital health [2], [3]. It encompasses a wide array of services, including remote condition and treatment monitoring, online specialist consultations and diagnoses, efficient storage and organization of patients' medical records, and online prescription of medication. Offering specialized medical care and guidance through mobile IoT systems is particularly advantageous for individuals living in rural or remote areas or for patients who cannot travel outside their homes.

The field of dermatology and the study of skin conditions and inflammation have not yet experienced significant advances in e-health and mobile monitoring [4]. Common skin diseases like atopic dermatitis (AD) still require in-person diagnosis and monitoring by a dermatologist at a hospital. Furthermore, in medical practices, there is no empirical method used to assess the condition, relying solely on the observation of the dermatologist, and there is no universally accepted treatment procedure, demonstrating again an inherent risk of subjectivity that can result in misdiagnosis or mistreatment [5], [6]. This emphasizes the necessity for a novel device that can remotely quantify the severity of the patient's condition, monitor its treatment for prolonged periods of time and ultimately be able to assist diagnosis of the disease. Such a device must be low-cost, compact, and non-invasive or wearable, to align with the daily routine of the patient.

Atopic dermatitis is a chronic skin condition, characterized by relapsing skin inflammation and pruritus (itchy skin),

This research was supported by DTP grant EP/T517859/1. The work of Stephen P Beeby was supported by the Royal Academy of Engineering under the Chairs in Emerging Technologies Scheme.

A. T., R.T, and S.B. are with the Faculty of Electronics and Computer Science, University of Southampton, SO17 1BJ, UK.

M. W is with the James Watt School of Engineering, University of Glasgow, G12 8QQ, UK.

K. G. and S. D. are with the Department of Biomedical Engineering, Rochester Institute of Technology, NY, US.

Data published in this article are available from the University of Southampton Repository at 10.5258/SOTON/D2893

which can cause the skin to appear red, swollen, scaled or vesiculated (have small vesicles on surface) [7]. There isn't a single confirmed factor contributing to the development of the disease, but it is widely accepted that it is due to a dysfunction in the outermost layer of the skin called the epidermis (EP), particularly in the disruption of the epithelial barrier, which is the main protective barrier against skin desiccation and environmental influences. The EP is composed of the stratum corneum (SC) and the viable epidermis (also known as stratum basale). The SC is where the epithelial barrier resides and it consists of tightly packed corneocyte cells, formed by skin keratin filaments enclosed within a protein envelope [8]. In healthy skin, these cells provide flexibility, durability, and resistance to tissue damage or diseases. In AD, the proteins responsible for regulating cellular adhesion and structure are deficient, which compromises the integrity of the barrier [9], [10]. This leads to an increase in water evaporation from the skin and subsequent severe dehydration of the outermost layer, a biomarker known as transepidermal water loss (TEWL). Fig. 1 visualizes the differences between healthy and AD skin – the breached barrier makes the skin more susceptible to environmental triggers such as allergens and microbes, which cause visual symptoms such as redness, irritation, and inflammation [11].

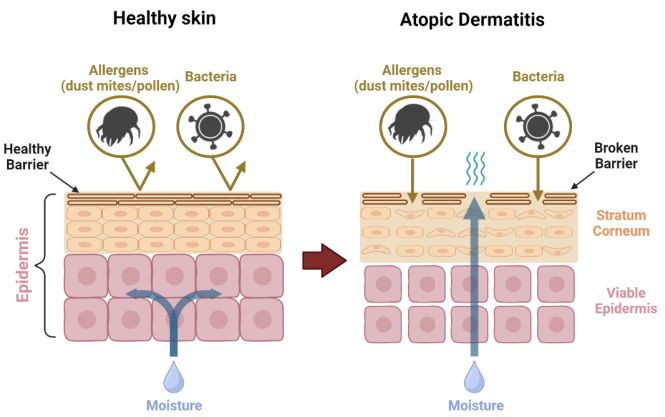

Fig. 1: Comparison of cellular structure in healthy skin versus skin with AD. Breaches in the skin barrier result in excessive water evaporation and a decrease in cell size.

There are methods that can be used to reduce subjectivity in the assessment of the severity of AD – from in vivo clinical examinations and tests to telemedical and non-invasive sensors for the different biomarkers of the condition, but none of them have been accepted as a medical practice within a diagnostic criterion for AD [12]–[20]. Furthermore, these methods all feature a trade-off between accuracy and mobility – as the most decisive of them, medical testing, does not fall in line with e-health and wearable technologies, and the ones that fulfill that criteria, telemedical sensors, lack the precision to be used for AD diagnosis. Todorov et al. have presented a comprehensive review of the topic, highlighting not only the current practices but also promising future technologies that can assist AD diagnosis [4].

Previous skin sensors in the literature are not optimized for quantifying AD biomarkers, because they consider the dielectric properties (permittivity) of the skin as a whole, rather than isolating detection of the outermost layers (SC and EP), where the AD biomarkers are present [16], [21]–[24]. The permittivity of the SC has not been empirically measured in the literature and the electric field penetration depth of current electrode skin sensors is rarely investigated, as there is no sensor designed specifically to measure within the outermost layers of the skin.

This paper presents a flexible sensor, designed specifically for the novel application of detecting biomarkers of AD, ultimately assisting in the empirical estimation of the severity of the condition and its distinction from other similar conditions. The biomarker in question is the dehydration of the outermost skin layers, caused by the escapement of water molecules through the broken SC barrier. The sensor monitors the dielectric properties of the skin using an interdigitated capacitor (IDC), which has been designed to increase the sensitivity while maintaining a penetration depth between the SC and the EP layers. Finite element analysis was used to confirm the validity of the electric field penetration depth. The simulated and experimental results verify the sensitivity to changes in hydration within the SC and the EP. The operation of the sensor and the simulation of its response is presented in section II. A unique skin phantom that mimics severely dry skin has also been developed to test the sensor, the fabrication of which is described in section III, alongside the experimental procedure and the manufacturing of the sensor itself. The sensor has been fabricated on a flexible substrate enabling ease of application on curved surfaces. The last sections present the results of the experiments along with a discussion and a future outlook on the field.

II. IDC Sensor Operation and Design

A. Operating Principle

Decreased water concentration within the SC and EP is a valid biomarker for the condition, as Martin et al. have correlated increased dryness and TEWL values to a decrease in size of the cells composing the SC barrier, and a lower concentration of water molecules below that barrier, in the EP [25]. The presence of free water molecules within the SC and the EP affects not only the chemical structure of the layers but also their dielectric properties. High water content in the SC increases the number of ionic pathways for electrons, by introducing more dipoles, thus enhancing the skin's response to applied electrical signals and elevating the amount of electrical energy that can be stored [26]. The SC layer can be thought of as a dielectric material, which when subjected to an electric field is polarized to a specific extent, determined by the permittivity and conductivity values. This can be empirically measured by circuit parameters such as resistance and capacitance, commonly grouped as complex impedance. Multiple studies have determined that skin exposed to moisturizing conditions exhibits reduced resistance and increased capacitance values compared to dry skin [15], [27]. Application of humectant or moisturizing cream enhances the skin's barrier properties, leading to an improved water retention within the SC, which is why it is commonly administered

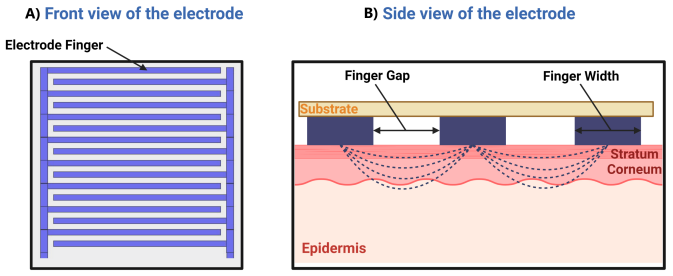

Fig. 2: Generic layout of the IDC sensor used. A) Plan view of the IDC, where an N number of electrode fingers are alternated in a particular pattern. B) Side view of the electrode with notation on the different components and terminology along with illustrative lines indicating the effect of the electric field. The Finger Gap (G) is the separation distance between neighboring electrode fingers and the Finger Width (FW) is the lateral width of a single electrode finger. Image not to scale.

as a remedy against symptoms of AD [25]. This study focuses on the drier spectrum, without the application of a humectant used in many other studies to elicit a response, to distinguish between AD and non-AD skin.

An interdigitated capacitive sensor is chosen as the measurement device, as its structure can be tailored to fit the specific needs of the study. It consists of two pairs of comb-patterned electrodes that are distanced by a specific gap – shown in Fig. 2 A). A cross-section of the electrode against the skin is presented in Fig. 2 B). An alternating electric field is applied to the skin by connecting one electrode to an alternating voltage source and grounding the other electrode. The penetration depth of the electric field must align with the depth of the SC and EP layers, which is around 25 – 150 µm, in order to achieve the highest sensitivity to dielectric changes within those layers [8]. General theory in the literature suggests that smaller gaps between electrodes result in shallower measurements [15], [28]–[30]. This is because at small electrode separation, most of the electric field lines penetrate at a depth close to the surface. Thus, the resistance and capacitance components of shallower layers have a greater effect, but there is little verification regarding that claim, so the authors have conducted finite element analysis on the design to explore the validity of the proposed sensor for monitoring AD.

B. Finite Element Analysis

COMSOL Multiphysics® software was used to perform Finite Element Analysis (FEA) of the sensor to explore the geometric factors for the purposes of this application. A sensor with a high sensitivity to changes in the SC and EP layers and a shallow penetration depth of around 25 – 150 µm was the goal of the study. A parametric sweep time stationary study with the electrostatics module was used with varying relative permittivities of the skin layers, simulating different hydration levels. A 3D model of a skin block with 3 layers (SC, EP, and dermis (DR)), was introduced. The thickness of each layer was 25, 150, and 1000 µm respectively, according to the literature [8]. To obtain values of the relative permittivity of the skin, the database presented by Gabriel et al. was used, which is the only study in the literature featuring frequency-coupled permittivity values for wet and dry skin [31]. Using the database in the region 1-100 kHz, values for extremely dry skin were extrapolated and were applied individually to each skin layer, following a method by Yao et al. [26]. The range of permittivity values used is presented in Table I, where the values of 1000 and 5000 were taken from Gabriel's database as the permittivity of normal dry (non-moisturized) and wetted (extra hydrated) skin at 1000 Hz, respectively. The extrapolated values for the relative permittivity of dry skin are therefore 100, 200, and 500.

TABLE I: DIMENSIONS AND PARAMETERS USED IN THE COMSOL SIMULATION ALONG WITH VALUES THEY TAKE DURING THE STUDIES

Dimension	Type	Value(s)
Relative Permittivity	Parameter	100, 200, 500, 1000, 2000, 5000
Gap (G)	Variable	100, 200, 800, 1600 µm
Finger Width (FW)	Variable	100, 200, 800, 1600 µm
Number of Fingers (N)	Variable	32, 16, 4, 2
Finger Length	Constant	6mm
Sensor Area	Constant	0.384 mm^2
Electrode Thickness	Constant	18 µm

The dimensions of the IDC affect the capacitance output and the penetration depth. To achieve consistency in the results the area of each IDC was kept constant, as the only varied parameters were the gap (G), the finger width (FW), and the number of fingers (N), which were changed proportionally. An IDC with G and FW both equal to 100 µm had 32 fingers; an IDC with G and FW both equal to 200 µm had 16 fingers and so on. The full set of simulated parameters is presented in order in Table I.

Copper was used as the electrode material and a 1 V harmonic perturbation signal was applied. The study was performed by varying the permittivity value (i.e. level of hydration) in the different layers and measuring the capacitance across the electrodes. When one skin layer's permittivity was varied, the other two were kept constant at 1000, and this study was performed for each of the different IDC sizes. The initial results agreed with the literature: the G100 N32 IDC and the G200 N16 IDC observed the highest change in capacitance per change in dielectric permittivity across the SC and EP layers. These two IDCs also showed the least sensitivity towards permittivity changes in the DR layer, indicating the effective measurement depth is shallower. The inverse behavior was observed when testing the larger gap IDCs. Fig. 3 A) and B) exemplify this relationship.

To further strengthen this argument, the intensity of the electric field along the z-axis inside the skin is measured as the permittivity of each layer is varied individually. The results from the G100 FW100 N32 IDC from the SC and the DR variation, presented in Fig. 4, clearly illustrate that there is no considerable effect on the electric field within the regions of interest (SC and EP) arising from changes in the DR. This means that a narrow gap IDC can serve as a measuring

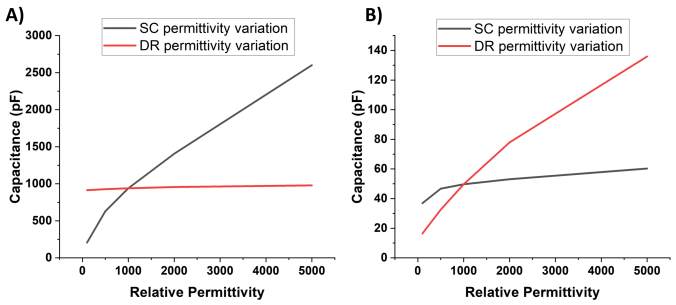

Fig. 3: Simulated capacitance versus relative permittivity of distinct skin layers (SC and DR) for: A) G100 FW100 N32 IDC sensor and B) G1600 FW1600 N2 IDC sensor.

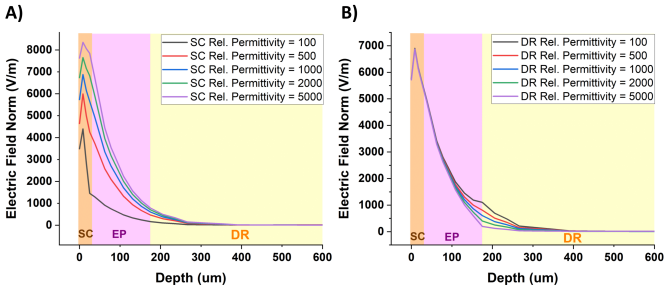

Fig. 4: Normalized electric field strength along the negative z-axis/depth of the skin medium for an G100 FW100 N32 IDC. The relative permittivity of A) the SC and B) the DR are subsequently varied to achieve a difference in response. A color map of the different skin layers is drawn following the thickness of each layer.

device for shallow depth hydration monitoring. Thus, the G100 FW100 N32 IDC was chosen as the most optimal design, tailored specifically for monitoring hydration in AD skin.

An analytical solution was also used to calculate the capacitance of the IDC using the relative permittivity values obtained from Gabriel's database [31]. The theoretical capacitance calculations also serve as closed-form validation for the COMSOL simulated capacitances. To perform the analysis, Angkawisittpan et al.'s formulae for the capacitance of an IDC were used and fitted following the notation of parameters so far [32]:

$$C = C_{UC}(N-1)L \tag{1}$$

$$C_{UC} = \epsilon_0(\frac{\epsilon_1+\epsilon_2}{2})\frac{K(\sqrt{1-k^2})}{K(k)} \tag{2}$$

$$k = \frac{G}{G+FW} \tag{3}$$

Here C_{UC} denotes the unit cell capacitance, or the capacitance between two neighboring electrode fingers; N is the number of fingers; L the length of single electrode finger; - the free space permittivity (8.854 x 10^{-12} F/m); ϵ_1 - the relative permittivity of the substrate (polyimide); ϵ_2 - the relative permittivity of the skin; and $K[x]$ is a complete elliptic integral of the first kind. An approximation can be made to shorten (2): since the permittivity of the skin is much larger than the permittivity of the substrate (around 3.5), the latter's component can be disregarded and thus (2) reduces to:

$$C_{UC} = \epsilon_0(\frac{\epsilon_{skin}}{2})\frac{K(\sqrt{1-k^2})}{K(k)} \tag{4}$$

Using (1), (3) and (4), and the parameters in I, the forward solution is calculated using MATLAB® software – obtaining capacitance values from relative permittivity/hydration variation. The value of 1000 was selected for the relative permittivity of the skin, as in Gabriel et al.'s database it is the value of normal (non-moisturized) skin [31]. The computed capacitance was 1083 pF for the G100 N32 IDC, 524 pF for G200 N16 IDC, and 58 pF for the G1600 N2 IDC, all of which were very close to the values obtained by the FEA simulation, thereby confirming its validity.

III. Methodology

A. Fabrication oF IDC

The IDC was manufactured by etching patterns from a copper-polyimide laminate sheet with copper thickness of 18 µm and polyimide thickness of 25 µm (GTS Flexible Materials Ltd, Gwent, United Kingdom), following a procedure described in Komolafe et al.'s paper [33], [34]. This substrate is low-cost, and the copper can easily be patterned using standard PCB etching techniques.

Three different IDC designs were fabricated, following the outcome of the FEA simulation in the previous section – a G100 FW100 N32 IDC, a G200 FW200 N16 IDC and a scaled-up version (bigger area) – G500 FW500 N10 IDC. The purpose of the last IDC is to feature a variation in the sensing area to confirm that boosting the capacitance output by increasing the area will not affect the sensitivity and the wider gap size of 500 µm would be more sensitive to the deeper layers. The first two sensors have an overall sensing area of 38.4 mm^2, whereas the last one has an area of 100 mm^2. Fig. 5 shows a photograph and an optical micrograph of the IDC.

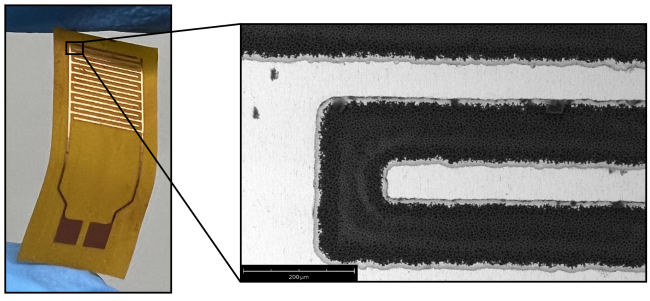

Fig. 5: Photograph and a micrograph taken using a scanning electron microscope. The flexibility of the fabricated IDC is presented in the photograph. The scale on the micrograph is 200 µm.

B. Skin Phantom Preparation

A novel replica of the skin, known as a skin phantom, is used to mimic the effects of severely dry skin. Skin phantoms

have been widely used in the literature to test electrode hydration sensors, but none of them replicate the drier spectrum of the skin, which is the focus of the phantom presented here. The phantom features two dielectric layers – the top one, named the SC layer, mimics the properties of a combined SC and EP and the bottom one replicates the DR layer. To control the level of dehydration within the SC layer, the porosity of this layer is varied by cutting a defined number of holes in it. The hydration control via porosity and the fabrication method are explained in detail and adapted from work by Goyal et al. [35]. The top SC layer has a thickness of 100 µm and it consists of a mixture of PDMS with 2.5% W/W carbon black powder to increase the conductivity, and 40% W/W Barium Titanate to increase the permittivity. The bottom DR layer has a thickness of 5 mm, and it is a PVA cryogel solution developed using 8.8 g of PVA powder mixed in 50 ml of 0.9% W/W saline solution (0.9 g of NaCl in 99.1 g of DI water). These specific mixtures create a soft and flexible phantom that closely resembles the structure of the skin. In the previous publication by Goyal, this phantom was measured to have an average impedance of 1 MΩ and 10 nF for low frequencies of 10–1000 Hz [35].

In this work, we implemented a hydration gradient across a single skin phantom by fabricating regions with different porosities but with the same underlying hydrated DR layer, so that the base is consistent among the tests and the variation relies solely on the SC layer. The different porosities each correspond to a state of dehydration. A 0% porosity SC layer means that there are no pores, the phantom is effectively a pure dielectric, and its behavior is only capacitive. In reality, skin can never be this dry and will always have some resistive properties, so this region on the phantom was produced to set the baseline. A 0.16% porosity SC layer represented very dry skin and a 0.28% porosity phantom resembled normal dry skin. The 0.16% porosity layer should approximate the dielectric behavior of skin with AD. Fig. 6 presents an illustration of the skin phantom.

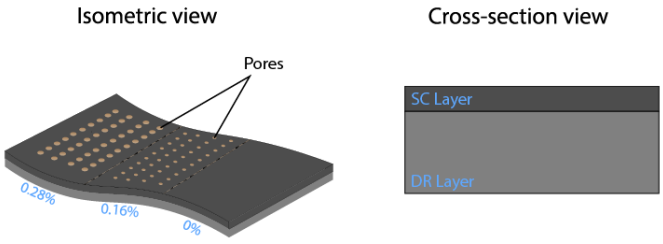

Fig. 6: Isometric and cross-sectional view of the novel fabricated hydration gradient skin phantom. The different hydration regions are labelled with their corresponding porosity. The layers of the phantom are labelled in the cross-sectional view with the SC layer replicating a combined SC and EP and the DR layer replicating DR and deeper tissues. The image and number of holes are not to scale.

C. Measurement Setup

To obtain impedance measurements from the IDCs, a Wayne-Kerr 6500B Impedance Analyzer was used across the two terminals of the IDC (Wayne Kerr Electronics, Bognor Regis, England). The IDCs were individually tested by being placed directly on top of the SC layer of the skin phantom, and a 5 N weight was placed on top to ensure constant pressure. The weight was made of PVA, an insulator, to ensure that it does not affect the readings. Fig. 7 depicts the experimental procedure – during testing the IDC was positioned with the electrodes in contact with the skin phantom and the weight was placed on top of the IDC. Five measurements on different sites on the phantom's surface were taken and an average value was calculated. Studies were conducted to source readings for impedance, phase, and capacitance for the frequency band of 100 Hz – 15 MHz.

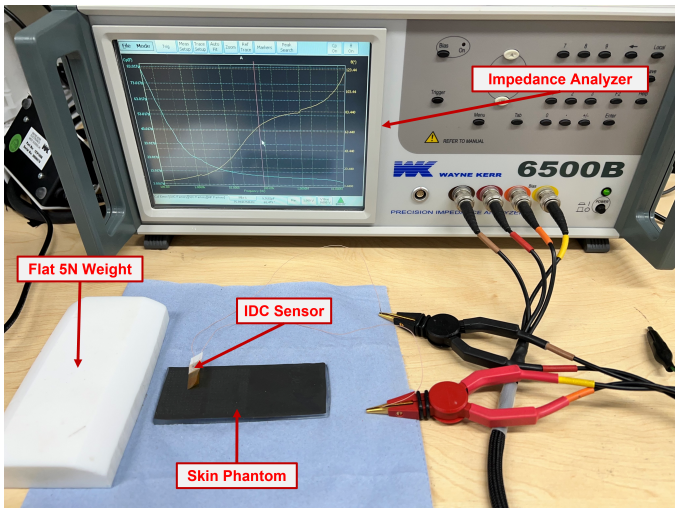

Fig. 7: Photograph of the experimental setup.

To verify the measurements, results were compared to a commercial skin hydration measurement device, a Corneometer® (Courage + Khazaka, Cologne, Germany). The Corneometer® is widely used as a validation for new hydration sensors and it is considered the gold standard for the field.

IV. Results and Discussion

The absolute value of complex impedance ($|Z|$) and phase (ϕ) of the IDCs were plotted against frequency for the different hydration states, expressed in porosity percentages. Figs. 8, 9 and 10 depict the plots of the G100 N32 IDC, the G200 N16 IDC, and the G500 N10 IDC, respectively. The impedance values were normalized with respect to area, to account for the dimension differences between the three IDCs. The phase plots of the 0% porosity for all the IDCs reveal a near positive 90 degrees, which means that the behavior is purely capacitive, and this is also confirmed by the linearity of the impedance. Therefore, the capacitive elements are prevalent in the complex response, thus measuring capacitance is a valid indicator for the performance of the IDC.

Across all devices a specific frequency is observed at which the different porosity plots converge. This frequency is around 100 kHz for the G100 IDC, close to 40 kHz for the G200 IDC, and 8 kHz for the G500 IDC. In the phase graphs, as the G size is increased, the phase plots shift towards the 0% porosity plot at 90°, and the frequency band, at which capacitive

properties dominate, is increased. The skin-sensor system can be fundamentally simplified to a resistor and capacitor in parallel. At lower frequencies there is resistive behavior arising from the ionic pathways of the water molecules, which allow for current to pass through easily, thereby decreasing the total impedance. This is visible in the impedance graphs, in the plots for 0.16% and 0.28% porosity on all IDCs. In the 0.28% porosity phantom, this effect is the strongest, because it is the most hydrated of all other phantoms. As the frequency is increased, this resistive effect disappears, and the skin becomes a pure capacitor. Therefore, to quantify the hydration of the outermost layers of the skin, an excitation signal with a frequency below this limit should be used.

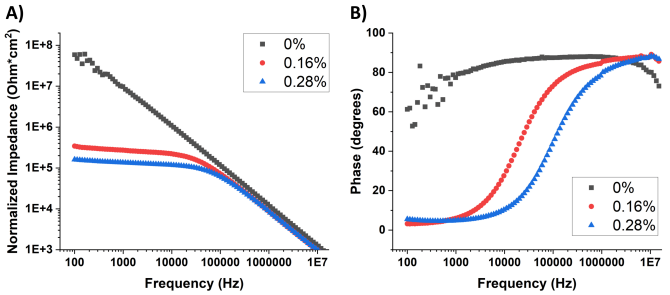

Fig. 8: Measurements for G100 FW100 N32 IDC at different porosity regions against frequency: A) Absolute value of complex impedance normalized and B) Phase in degrees. Porosity values are expressed in percentages and correspond to extremely dehydrated (0%), dehydrated (0.16%) and normal (0.28%) SC layer.

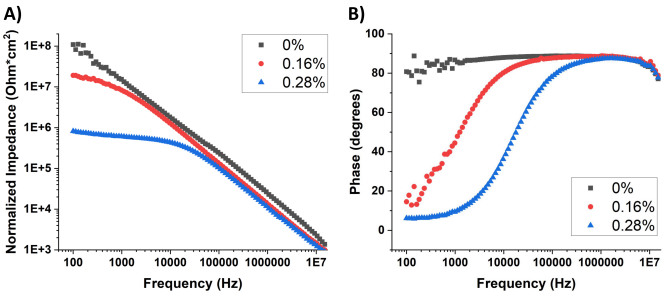

Fig. 9: Measurements for G200 FW200 N16 IDC at different porosity regions against frequency: A) Absolute value of complex impedance normalized and B) Phase in degrees. Porosity values are expressed in percentages and correspond to extremely dehydrated (0%), dehydrated (0.16%) and normal (0.28%) SC layer.

As it was discovered in the COMSOL simulation, the gap size of the IDCs affects the penetration depth the most, and that is also visible in the impedance plots here. The G500 IDC is more influenced by the deeper PVA layer of the phantom, that is why changes in the SC layer introduce little resistive effect on the total impedance (Fig. 10A). In contrast, for the G100 IDC, there is a considerable spread between the impedance values of the different porosity states, because it is most sensitive to changes in the SC layer. The capacitance

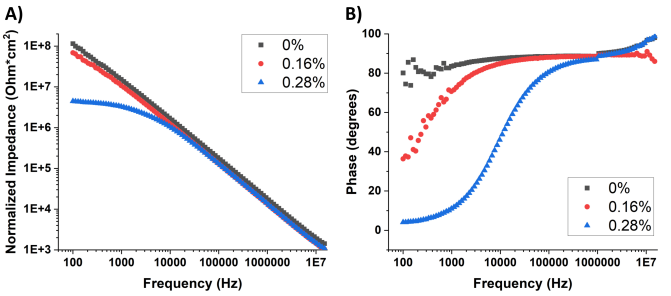

Fig. 10: Measurements for G500 FW500 N10 IDC at different porosity regions against frequency: A) Absolute value of complex impedance normalized and B) Phase in degrees. Porosity values are expressed in percentages and correspond to extremely dehydrated (0%), dehydrated (0.16%) and normal (0.28%) SC layer.

versus frequency for the different porosity states is plotted for all IDCs in Fig. 11. The same area normalization was applied as with the complex impedance, and the graphs are plotted in separate windows because of the exponential difference in the measurements for the G100 N32 IDC and the other two IDCs.

The capacitance plots agree with the conclusion that the G100 IDC is the best design as it provides the highest sensitivity and achieves a measurement depth to distinguish dehydration levels of the SC. The G200 and the G500 IDC do show increasing capacitance values for the 0.28% porosity region versus frequency, but they cannot distinguish between the other two porosity levels. Given the plots, the frequency band around 1 kHz is a reasonable value for the excitation signal, as the capacitance exhibits the highest sensitivity to different hydration states.

To validate the sensor's capacitance readings, the measured capacitance of the different IDC sizes at 1 kHz were compared to the hydration readings of the Corneometer®, which is a commercial skin hydration device. It yields hydration readings in arbitrary units (A.U.) and was used to measure the skin phantom's hydration - the comparison is presented in Fig. 12. From the graph, all IDCs follow the trend of increasing capacitance with hydration level. The sensitivity of the individual IDCs can be mapped against that of the Corneometer®, by dividing the change in capacitance of the IDCs between hydration levels by the change in A.U. of the Corneometer® between the same levels. The formula used is presented in Eq. (5):

$$S = \frac{\Delta C}{\Delta H} \tag{5}$$

where ΔH is difference in the commercial sensor's responses for different hydration levels. This results in a sensitivity of 13.1 pF/cm^2 per 1 A.U. for the G100 IDC, 6.08 pF/cm^2 per 1 A.U. for the G200 IDC, and 0.38 pF/cm^2 per 1 A.U. for the G500 IDC. The G100 IDC demonstrates a higher sensitivity towards changes in the SC hydration than the other IDCs, and therefore it is the most optimal for the purposes of AD monitoring.

To equate the impedance and capacitance readings to rel-

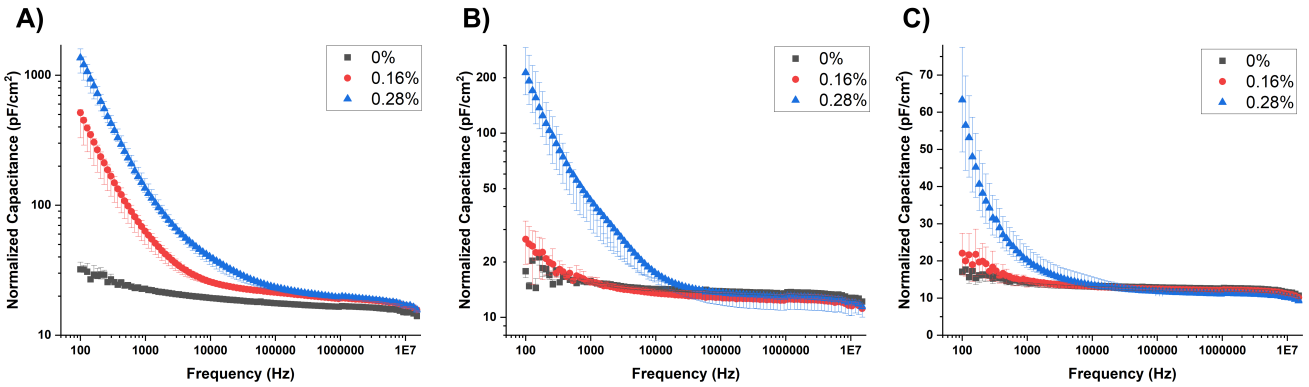

Fig. 11: Measurements for the normalized capacitance against frequency at the different porosity phantoms of a: A) G100 FW100 N32 IDC; B) G200 FW200 N16 IDC; C) G500 FW500 N10 IDC. Porosity values are expressed in percentages and correspond to extremely dehydrated (0%), dehydrated (0.16%) and normal (0.28%) SC layer.

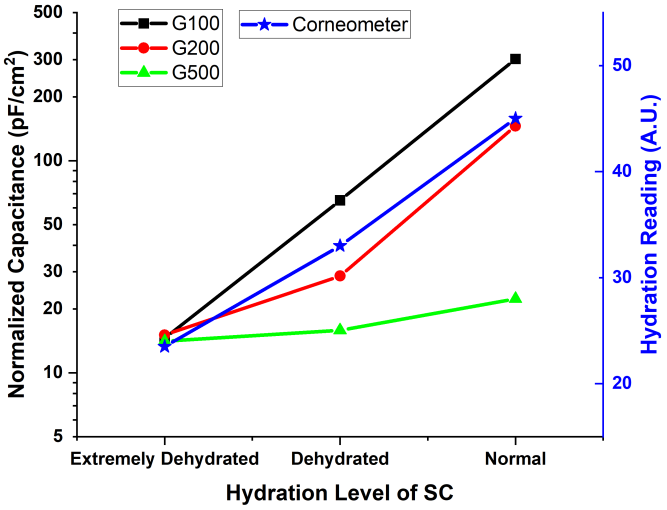

Fig. 12: Capacitance readings from different IDCs explored in this paper and hydration readings from Corneometer® against the three different hydration levels of the SC, achieved by the hydration gradient skin phantom.

ative permittivity values, the analytical approach was again used. Following Eq. (1), (3), and (4), the inverse solution was input in MATLAB to calculate relative permittivity values or hydration states from capacitance readings from the experiments. The readings from the 0.28% porosity region were taken, which would equate to normal SC hydration. The capacitance of both the G100 and the G200 IDC at 1 kHz were much lower than the simulations – around 126 pF and 59 pF, respectively, so the computed relative permittivities were also lower – 116 and 110, which is very different from Gabriel et al.'s values. In the initial conditions of the analysis, it was stated that those values were not for the SC layer specifically, but rather for the skin as a single block. There are other sources in the literature claiming that the relative permittivity of individual SC cells is around 86 – 90 but have not proven it empirically [36]. Thus, Gabriel et al.'s database might not be applicable or appropriate for the purposes of this study.

Finally, a stepwise response investigation was undertaken to determine the behavior of the sensor when placed on and off the phantom. Parameters such as the response and recovery times provide more insight into the operation of the sensor. For this test only the G100 IDC was used, since it was discovered to be optimal for the purposes of SC hydration sensing. The test conducted was to repeatedly press and release a single G100 IDCs onto the different porosity areas of the hydration gradient phantom whilst continuously sampling capacitance data from the impedance analyzer every 0.2 seconds with the help of a LabView® script. The testing procedure was distributed as follows: 5 seconds off-time (no contact to skin phantom, the sensor is in the air), followed by 5 seconds on-time (pressed to the skin phantom with the same 5 N weight as used before), 5 seconds off. This was repeated with each of the 3 different porosity sections tested 2 times during the 75-second test. The results are shown in Fig. 13.

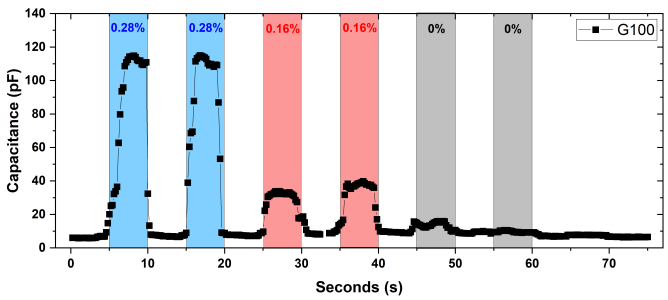

Fig. 13: Step-response of a G100 N32 IDC sensor on a hydration-gradient skin phantom with 3 porosity levels. Excitation signal of the impedance analyzer was 1 V at 1 MHz.

As expected, the readings match the frequency sweep measurements at the given frequency band (1 MHz) and the distinction between the different porosity levels is evident – indicating that even at 1 MHz excitation frequency the sensor can distinguish various SC hydration levels. Using the stepwise response graph, the parameters of response and recovery times can be calculated. For the first period in contact with the 0.28% porosity phantom, the capacitance begins increasing first slowly, then more rapidly and it rises from around 9.3 pF to 108.6 pF in 2.4 seconds. This is a response

of about 41.4 pF/s when in transition between air and normally hydrated skin. The following recovery time is much faster – it goes from 110.9 pF to 8 pF in 0.6 s, which is a recovery time of 171.5 pF/s. During the second period in contact with the 0.28% porosity phantom, the response time is much faster, 85.4 pF/s, whereas the recovery time is approximately the same. For the two contact periods with the 0.16% porosity the response and recovery times are close to each other at around 26 pF/s, but that is expected since this is replicating the drier spectrum of skin hydration. The stepwise response shows stable and repeatable operation when performing quick sampling measurements using the IDC sensor on the skin phantom.

V. External Variables Test

A. Effect of Environmental Humidity

To fully understand the measurements of the IDC sensor, the possible effect of environmental humidity must be investigated. Since the IDC is sensitive to the presence of water molecules in the media it is measuring, environments with high humidity should have an effect on the IDC, thus increasing the capacitance readings. All the produced IDCs in this work were individually tested inside a climate chamber (WKL 100, Weiss Technik) and their capacitance was continuously sampled every 30 seconds using the Wayne Kerr 6500B Impedance Analyzer and a LabView® script for 20 minutes while the chamber's humidity was raised linearly from 50% (relative humidity of room) to 95%. The excitation signal from the impedance analyzer was the same as used in the initial capacitance testing – 1 V at 1 kHz. Temperature was kept the same throughout the measurements at 25ºC. Results are portrayed in Figs. 14, 15, and 16.

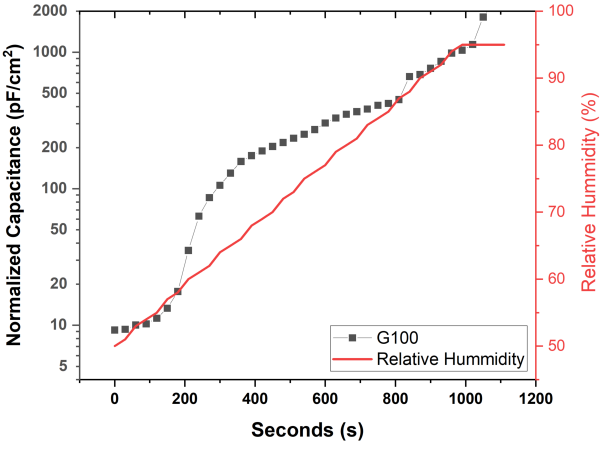

Fig. 14: Capacitance versus time for a G100 N32 IDC sensor placed inside an environmental chamber with varying relative humidity between 50% and 95%.

In all graphs, it is evident how the capacitance increases by several orders of magnitude due to the increase of relative humidity above a certain threshold. For the G100 and the G500 that threshold is about 60%, and for the G200 it is about 70%. This shows the sensors have a working range of 40-60% relative humidity, which is consistent with typical

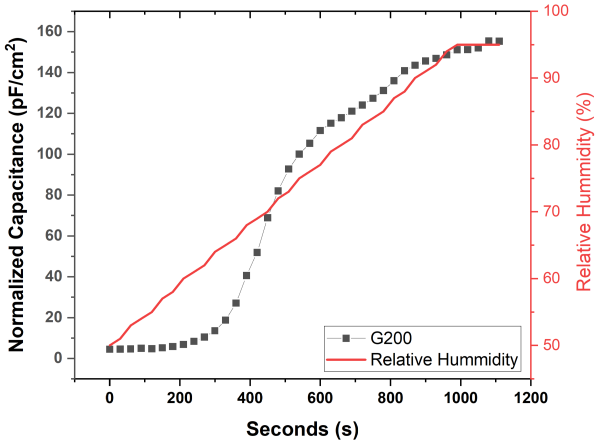

Fig. 15: Capacitance versus time for a G200 N16 IDC sensor placed inside an environmental chamber with varying relative humidity between 50% and 95%.

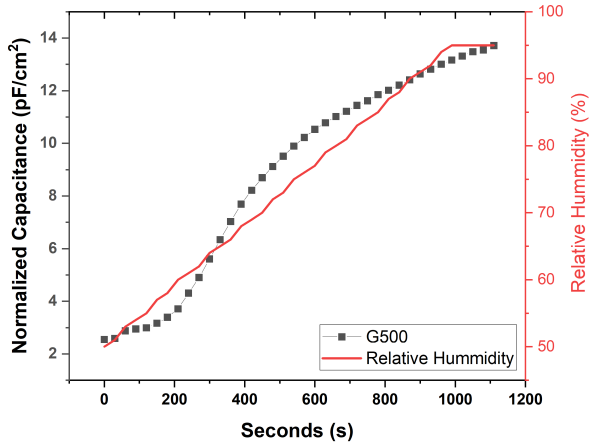

Fig. 16: Capacitance versus time for a G500 N10 IDC sensor placed inside an environmental chamber with varying relative humidity between 50% and 95%.

room conditions. After this threshold is passed, there is an initial sharp increase in capacitance, visible in the G200 and G100 plots, after which the gradient changes. In the later stages of the humidity test on the G100 IDC, around the 800^{th} and 1100^{th} seconds, there is a sharp increase that almost doubles the capacitance. Since these all occur at high humidity, it is believed that this is caused by condensation of water molecules onto the surface of the IDC. The G100 IDC has the smallest separation distance between the electrodes and is most sensitive to changes in the dielectric medium arising from water molecules forming on the sensor. After the testing was finished, and the sensors were brought back to normal room humidity all of them returned to their original capacitance values. Unlike the G200 and the G500, the G100 IDC's capacitance values remained high for a long period of time after testing ended. To increase the range of humidities the sensor can function over and mitigate condensation effects a possible solution would be to implement an encapsulation layer, but that would decrease the sensitivity and offset the measurement depth.

B. Effect of Environmental Temperature

Similarly to humidity, the effect of temperature on the capacitance readings of the sensor is also investigated. The IDCs sensors were again placed individually inside an oven and the temperature was gradually increased from 25ºC to 100ºC while keeping average room relative humidity at 50%. Testing took 20 minutes, and data was sampled every 1 minute using a Wayne Kerr 6500b Impedance Analyzer with an excitation signal of 1 V at 1 kHz and a LabView® script. Results are on Fig. 17.

As it is seen on the graph, the effect of temperature on the IDCs readings is negligible compared to the range of readings when comparing different hydration levels. In the G100 and G200 IDCs there is a slight decrease in readings before stabilizing, which is attributed to evaporation of any residual water molecules that might be present on the surface of the sensor from the ambient air humidity.

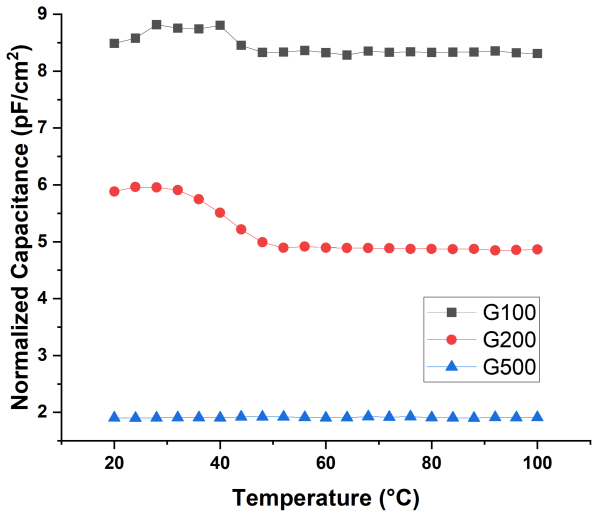

Fig. 17: Normalized capacitance versus temperature for 3 types of IDCs: G100 N32, G200 N16 and G500 N10. The capacitance values were normalized to account for the area differences between the IDC sensors.

C. Effect of Bending

The effect of bending radius is also investigated as an external variable since the IDCs are printed on a flexible substrate. The same impedance analyzer setting was used as with the previous external variables testing (1 V at 1 kHz). Three different cylinders with varying radii of 15 mm, 10 mm and 5 mm were 3D printed from PLA and the IDC sensor was bent around the cylinders with the electrodes facing outwards. Given that the length of the G100/G200 IDCs is around 6.4 mm and that of the G500 is 10 mm, the smallest radius would cause a total bend of approximately 90º. As PLA and Kapton are both polymers with comparable dielectric permittivity, this would introduce no capacitance changes, so any variations in capacitance should arise from the effect of the sensor being bent. The results in Figure 18 reveal that there is no significant effect of bending radii on the capacitance of the IDC in air and hence the IDCs can effectively be used in wearable applications where bending may occur in use.

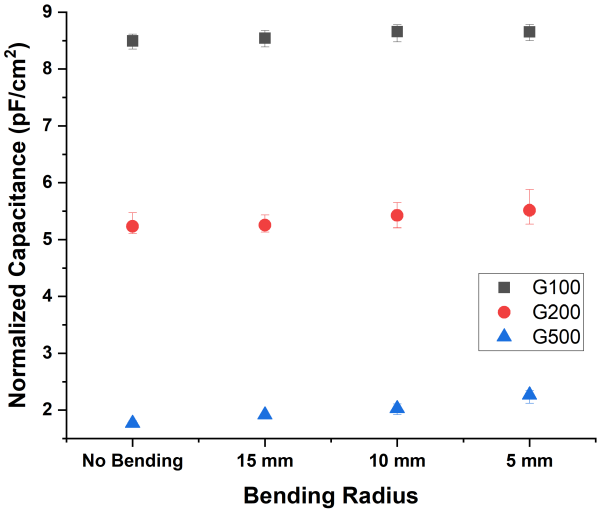

Fig. 18: Normalized capacitance versus bending radii for 3 different IDC sensors (G100 N32, G200 N16 and G500 N10). Several tests were conducted, and the average value was taken; error bars indicate the range of values obtained.

VI. Conclusion

A novel IDC sensor has been presented, tailored for the application of monitoring AD biomarkers, and its behavior is characterized and optimized to fit the purposes of the study. The optimal sensor features 32 electrode fingers of width 100 µm, spaced by 100 µm gaps. The sensor can distinguish between different levels of dehydration of the SC layer, where the condition is mostly prevalent and therefore it can help in estimating the severity of the condition or monitor its treatment. This is the first electrode sensor created for the purposes of examining AD skin and the first to prove its increased sensitivity towards a specific layer of the skin and could be used to allow health practitioners to track the condition of the patients remotely, without the need of examination in a health clinic. Alongside the IDC sensor, a novel hydration gradient skin phantom has been demonstrated to calibrate the sensor's measurements. The skin phantom offers a common basis for testing future devices for AD skin, as it achieves varying SC hydration levels on the same substrate, useful for determining disease severity across several points on the skin, as atopic skin is often composed of patches of dehydrated and irritated skin next to normal skin. The proposed IDC can be easily scaled to fit the application, as areal scaling doesn't affect the sensitivity for a fixed spacing between interdigitated electrodes. Its low footprint and ease of fabrication render it a usable device to be embedded in a mobile or wearable system. Further work would entail the development of a micro-based system using an impedance analyzing circuit and a data-processing MCU for measurement selection based on the findings of this paper: frequency scope between 1 kHz – 1 MHz and room humidity between 40-60%. Future work will also investigate how cross-sensitivities can be mitigated

using additional sensors and potentially the use of machine learning. Ultimately, the finished system will be tested on human patients with AD to determine its efficacy in monitoring the condition.

REFERENCES

[1] S. C. Mukhopadhyay, "Wearable sensors for human activity monitoring: A review," *IEEE Sensors Journal*, vol. 15, no. 3, pp. 1321–1330, 2015.

[2] M. M. Rodgers, V. M. Pai, and R. S. Conroy, "Recent advances in wearable sensors for health monitoring," *IEEE Sensors Journal*, vol. 15, no. 6, pp. 3119–3126, 2015.

[3] L.-Y. Ma and N. Soin, "Recent progress in printed physical sensing electronics for wearable health-monitoring devices: A review," *IEEE Sensors Journal*, vol. 22, no. 5, pp. 3844–3859, 2022.

[4] A. Todorov, R. Torah, M. R. Ardern-Jones, and S. P. Beeby, "Electromagnetic sensing techniques for monitoring atopic dermatitis—current practices and possible advancements: A review," *Sensors*, vol. 23, no. 8, p. 3935, 2023.

[5] D. De, A. J. Kanwar, and S. Handa, "Comparative efficacy of hanifin and rajka's criteria and the uk working party's diagnostic criteria in diagnosis of atopic dermatitis in a hospital setting in north india," *Journal of the European Academy of Dermatology and Venereology*, vol. 20, no. 7, pp. 853–859, 2006.

[6] E. E. A. Brenninkmeijer, M. E. Schram, M. M. G. Leeflang, J. D. Bos, and P. I. Spuls, "Diagnostic criteria for atopic dermatitis: a systematic review," *British Journal of Dermatology*, vol. 158, no. 4, pp. 754–765, 2008.

[7] A. O. Rinaldi, A. Korsfeldt, S. Ward, D. Burla, A. Dreher, M. Gautschi, B. Stolpe, G. Tan, E. Bersuch, D. Melin, N. Askary Lord, S. Grant, P. Svedenhag, K. Tsekova, P. Schmid-Grendelmeier, M. Möhrenschlager, E. D. Renner, and C. A. Akdis, "Electrical impedance spectroscopy for the characterization of skin barrier in atopic dermatitis," *Allergy*, vol. 76, no. 10, pp. 3066–3079, 2021.

[8] J. A. Bouwstra, P. L. Honeywell-Nguyen, G. S. Gooris, and M. Ponec, "Structure of the skin barrier and its modulation by vesicular formulations," *Progress in Lipid Research*, vol. 42, no. 1, pp. 1–36, 2003.

[9] S. Reitamo, T. A. Luger, and M. Steinhoff, *Textbook of Atopic Dermatitis*. Informa Healthcare, 2008.

[10] C. N. A. Palmer, A. D. Irvine, A. Terron-Kwiatkowski, Y. Zhao, H. Liao, S. P. Lee, D. R. Goudie, A. Sandilands, L. E. Campbell, F. J. D. Smith, G. M. O'Regan, R. M. Watson, J. E. Cecil, S. J. Bale, J. G. Compton, J. J. DiGiovanna, P. Fleckman, S. Lewis-Jones, G. Arseculeratne, A. Sergeant, C. S. Munro, B. E. Houate, K. McElreavey, L. B. Halkjaer, H. Bisgaard, S. Mukhopadhyay, and W. H. I. McLean, "Common loss-of-function variants of the epidermal barrier protein filaggrin are a major predisposing factor for atopic dermatitis," *Nature Genetics 2006 38:4*, vol. 38, no. 4, pp. 441–446, 2006.

[11] I. Nicander and S. Ollmar, "Clinically normal atopic skin vs. non-atopic skin as seen through electrical impedance," *Skin Research and Technology*, vol. 10, no. 3, pp. 178–183, 2004.

[12] R. M. Herd, M. J. Tidman, R. J. Prescott, and J. A. A. Hunter, "The cost of atopic eczema," *British Journal of Dermatology*, vol. 135, no. 1, pp. 20–23, 1996.

[13] I. Wessler, T. Reinheimer, H. Kilbinger, F. Bittinger, C. J. Kirkpatrick, J. Saloga, and J. Knop, "Increased acetylcholine levels in skin biopsies of patients with atopic dermatitis," *Life Sciences*, vol. 72, no. 18-19, pp. 2169–2172, 2003.

[14] M. Akdeniz, S. Gabriel, A. Lichterfeld-Kottner, U. Blume-Peytavi, and J. Kottner, "Tewl reference values in healthy adults," *British Journal of Dermatology*, vol. 179, no. 5, pp. e204–e204, 2018.

[15] M. A. Yokus and M. A. Daniele, "Skin hydration sensor for customizable electronic textiles," *MRS Advances*, vol. 1, no. 38, pp. 2671–2676, 2016.

[16] M. Jang, H.-D. Kim, H.-J. Koo, and J.-H. So, "Textile-based wearable sensor for skin hydration monitoring," *Sensors*, vol. 22, no. 18, p. 6985, 2022.

[17] Y. Noro, Y. Omoto, K. Umeda, F. Tanaka, Y. Shiratsuka, T. Yamada, K. Isoda, K. Matsubara, K. Yamanaka, E. C. Gabazza, M. Nishikawa, and H. Mizutani, "Novel acoustic evaluation system for scratching behavior in itching dermatitis: Rapid and accurate analysis for nocturnal scratching of atopic dermatitis patients," *The Journal of Dermatology*, vol. 41, no. 3, pp. 233–238, 2014.

[18] K. Pan, G. Hurault, K. Arulkumaran, H. C. Williams, and R. J. Tanaka, *EczemaNet: Automating Detection and Severity Assessment of Atopic Dermatitis*, pp. 220–230. Springer International Publishing, 2020.

[19] R. Schiavoni, G. Monti, E. Piuzzi, L. Tarricone, A. Tedesco, E. De Benedetto, and A. Cataldo, "Feasibility of a wearable reflectometric system for sensing skin hydration," *Sensors 2020, Vol. 20, Page 2833*, vol. 20, no. 10, pp. 2833–2833, 2020.

[20] N. Petitdidier, A. Koenig, R. Gerbelot, H. Grateau, S. Gioux, and P. Jallon, "Contact, high-resolution spatial diffuse reflectance imaging system for skin condition diagnosis," vol. 23, no. 11, pp. 115003–115003, 2018.

[21] B. Yang and Y. Dong, "A portable dual-parameter tester for assessing electrical properties of human skin surface," *IEEE Sensors Journal*, vol. 16, no. 2, pp. 426–435, 2016.

[22] X. Huang, C. Huanyu, C. Kaile, Z. Yilin, Z. Yihui, L. Yuhao, Z. Chenqi, O. Shao-chi, K. Gil-Woo, Y. Cunjiang, H. Yonggang, and J. A. Rogers, "Epidermal impedance sensing sheets for precision hydration assessment and spatial mapping," *IEEE Transactions on Biomedical Engineering*, vol. 60, no. 10, pp. 2848–2857, 2013.

[23] R. Matsukawa, A. Miyamoto, T. Yokota, and T. Someya, "Skin impedance measurements with nanomesh electrodes for monitoring skin hydration," *Advanced Healthcare Materials*, vol. 9, no. 22, pp. 2001322–2001322, 2020.

[24] J. Balaban and T. Blecha, "Textile sensor for skin hydration measurement," IEEE.

[25] K. Martin, "In vivo measurements of water in skin by near-infrared reflectance," vol. 52, no. 7, pp. 1001–1007, 2016.

[26] S. Yao, A. Myers, A. Malhotra, F. Lin, A. Bozkurt, J. F. Muth, Y. Zhu, S. Yao, A. Myers, Y. Zhu, A. Malhotra, F. Lin, A. Bozkurt, and J. F. Muth, "A wearable hydration sensor with conformal nanowire electrodes," *Advanced Healthcare Materials*, vol. 6, no. 6, pp. 1601159–1601159, 2017.

[27] S. Björklund, T. Ruzgas, A. Nowacka, I. Dahi, D. Topgaard, E. Sparr, and J. Engblom, "Skin membrane electrical impedance properties under the influence of a varying water gradient," *Biophysical Journal*, vol. 104, no. 12, pp. 2639–2650, 2013.

[28] L. Q. Jun, G. W. bin Djaswadi, H. F. bin Hawari, and M. A. B Zakariya, "Simulation of interdigitated electrodes (ides) geometry using comsol multiphysics," in *2018 International Conference on Intelligent and Advanced System (ICIAS)*, pp. 1–6, IEEE.

[29] D. F, F. L, C. A, and T. M, "Optimization of skin impedance sensor design with finite element simulations," in *COMSOL Conference*.

[30] N. Zoric, "Design and simulations of idc sensor using comsol multyphysics and dielectric spectroscopy of ltcc spectroscopy of ltccmaterials," 2013.

[31] S. Gabriel, R. W. Lau, and C. Gabriel, "The dielectric properties of biological tissues: Iii. parametric models for the dielectric spectrum of tissues," *Physics in Medicine and Biology*, vol. 41, no. 11, pp. 2271–2293, 1996.

[32] N. Angkawisittpan and T. Manasri, "Determination of sugar content in sugar solutions using interdigital capacitor sensor," *Measurement Science Review*, vol. 12, no. 1, 2012.

[33] A. Komolafe, R. Torah, Y. Wei, H. Nunes-Matos, M. Li, D. Hardy, T. Dias, M. Tudor, and S. Beeby, "Integrating flexible filament circuits for e-textile applications," *Advanced Materials Technologies*, vol. 4, no. 7, p. 1900176, 2019.

[34] G. F. M. Ltd., "Gts 7800 - copper polyimide laminates, gts ultraflex datasheet," 1999.

[35] K. Goyal, D. A. Borkholder, and S. W. Day, "A biomimetic skin phantom for characterizing wearable electrodes in the low-frequency regime," *Sensors and Actuators A: Physical*, vol. 340, pp. 113513–113513, 2022.

[36] L. Davies, P. Chappell, and T. Melvin, "Modelling the effect of hydration on skin conductivity," *Skin Research and Technology*, vol. 23, no. 3, pp. 363–368, 2017.

Alexandar R. Todorov received his B.Eng. (Hons.) in Mechatronic Engineering in 2021 from the University of Southampton. His undergraduate research involved energy harvesting solutions for wearable electronics and e-textiles.

He is currently pursuing his Ph.D. in Electrical and Electronic Engineering as part of the Smart Electronic Materials and Systems research group at the University of Southampton. The topic of his research is investigation and development of bespoke healthcare monitoring sensors for wearable applications. His research interest involves on-body energy harvesting, non-invasive medical sensing for enabling e-health technologies, and integration of transducers in wearable applications.

Krittika Goyal is currently working as a Visiting Lecturer in Manufacturing and Mechanical Engineering Technology at RIT (Rochester, NY, USA). She received her PhD in Microsystems Engineering from Rochester Institute of Technology in 2023. Her research deals with improving the signal quality from dry electrodes to overcome the challenges of in-home physiological monitoring devices. Her research interests include biomedical instrumentation, sensors and transducers, non-invasive physiological measurements, and their computational modeling. She received her Bachelor's (BE) and Master's (ME) degree in Electronic Instrumentation and Control from Thapar University, Patiala, India in 2016.

Russel Torah received the B.Eng. degree (Hons.) in electronic engineering, the M.Sc. degree in instrumentation and transducers, and Ph.D. degree in electronics with a focus on the optimization of thick-film piezoceramics from the University of Southampton, in 1999, 2000, and 2004, respectively. Since 2005, he has been a full-time Researcher with the University of Southampton, where he is currently a Principal Research Fellow. His current research interest includes smart fabric development, but he also has extensive knowledge of energy harvesting, sensors, and transducers. He has more than 50 publications in this field).

Mahmoud Wagih (GS'18, M'21) received his B.Eng. (Hons.) in September 2018, and his Ph.D. on rectenna design in April 2021, both in Electrical and Electronic Engineering from the University of Southampton.

He is currently a UK IC Research Fellow and Proleptic Lecturer (Assistant Professor) at the University of Glasgow. His interests broadly RF and antenna-enabled sustainable electronics including energy harvesting, sensing, and wearable applications.

Michael R. Ardern-Jones was appointed to University Hospitals Southampton NHS Trust and to the Faculty of Medicine, University of Southampton in 2007.

He has a specific academic interest in inflammatory skin disease and leads the clinical service for eczema, skin allergy and drug hypersensitivity reactions. At a national level he has previously served as President of the British Society for Medical Dermatology, Chair of the British Society for Investigative Dermatology, chair of The Skin Investigation Society. As well as continuing clinical practice, and running a research lab, he is currently the Wessex Dermatology Research lead for clinical trials, Vice President of the British Association of Dermatologists (Academic) and is an advisor to UK Government (NICE and MHRA).

Steven W. Day is the Harvey J Palmer Professor of Biomedical Engineering at RIT (Rochester, NY, USA). His research deals with the application of computational mechanics to a range of applied medical and biological problems. This includes collaborations with biologists, medical doctors, and industry partners. Prof. Day hold a BS degree in mechanical engineering and PhD in mechanical and aerospace engineering from the University of Virginia, as well as a diploma from the von Karman Institute for Fluid Dynamics. He is faculty of the Kate Gleason College of Engineering at RIT since 2004, and Department Head of Biomedical Engineering since 2016.

Prof. Beeby obtained his Ph.D. from the University of Southampton, UK, in 1998 on the subject of MEMS resonant sensors. He has been awarded two EPSRC Research Fellowships to investigate the combination of screen-printed active materials with micromachined structures and textiles for energy harvesting. He was awarded a personal Chair in 2011. His research interests include energy harvesting, e-textiles, MEMS, and active printed materials development. He leads the UK's E-Textiles Network and is Chair of the International Steering Committee for the PowerMEMS and E-Textiles conferences.